

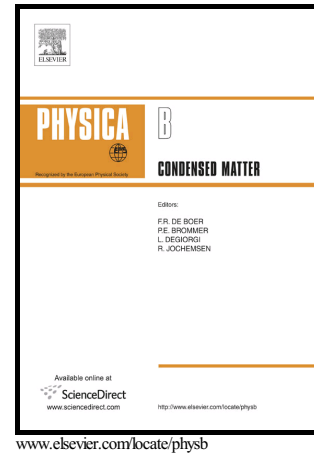
This is the Post-print version of the following article: *F. López-Urías, J.J. Torres-Heredia, E. Muñoz-Sandoval, Cobalt double-ring and double-dot structures: Magnetic properties, Physica B: Condensed Matter, Volume 483, 2016, Pages 62-68*, which has been published in final form at: <https://doi.org/10.1016/j.physb.2015.12.026>

© 2016. This manuscript version is made available under the CC-BY-NC-ND 4.0 license <http://creativecommons.org/licenses/by-nc-nd/4.0/>

Author's Accepted Manuscript

Cobalt Double-Ring and Double-Dot Structures: Magnetic Properties

F. López-Urías, J.J. Torres-Heredia, E. Muñoz-Sandoval



PII: S0921-4526(15)30358-6
DOI: <http://dx.doi.org/10.1016/j.physb.2015.12.026>
Reference: PHYSB309293

To appear in: *Physica B: Physics of Condensed Matter*

Received date: 24 September 2014
Revised date: 7 December 2015
Accepted date: 14 December 2015

Cite this article as: F. López-Urías, J.J. Torres-Heredia and E. Muñoz-Sandoval Cobalt Double-Ring and Double-Dot Structures: Magnetic Properties, *Physica B Physics of Condensed Matter*, <http://dx.doi.org/10.1016/j.physb.2015.12.026>

This is a PDF file of an unedited manuscript that has been accepted for publication. As a service to our customers we are providing this early version of the manuscript. The manuscript will undergo copyediting, typesetting, and a review of the resulting galley proof before it is published in its final citable form. Please note that during the production process errors may be discovered which could affect the content, and all legal disclaimers that apply to the journal pertain

Cobalt Double-Ring and Double-Dot Structures: Magnetic Properties

F. López-Urías^{1*}, J. J. Torres-Heredia², E. Muñoz-Sandoval¹

¹Advanced Materials Department, IPICYT, Camino a la presa San José 2055, Col. Lomas 4a sección, 78216, San Luis Potosí S.L.P., México.

²Instituto Tecnológico Superior de Las Choapas, Col. J. M. Rosado, 96980, Las Choapas, Veracruz; Mexico.

*To whom correspondence should be addressed: flo@ipicyt.edu.mx

Tel: +52 (444) 834-2000 (ext. 7238); Fax: +52 (444) 834-2000.

Abstract

The magnetization reversal mechanism of nanostructures of cobalt double-rings (D-rings) and double-dots (D-dots) is investigated in the framework of micromagnetic simulations. The arrays contain two identical coupled rings (wide and narrow) or dots with outer diameter of 200 nm and thicknesses ranging from 2-20 nm. Hysteresis loops, dipole-dipole and exchange energies are systematically calculated for the cases of the structures touching and the structures with a 50-nm inter-magnet separation; moreover, magnetization states along the hysteresis curve are analyzed. The results of both dot and ring D-magnets are compared with the corresponding individual magnets. Our results reveal that all D-ring (in contact and separated) arrays containing narrow rings exhibit non-null remanent magnetization; furthermore, higher coercive fields are promoted when the magnet thickness is increased. It is observed that the magnetization reversal is driven mainly by a clockwise rotation of onion-states, followed by states of frustrated vortices. Our results could help improve the understanding of the magnetic interactions in nanomagnet arrays.

Keywords: Nanorings, nanodots, double-nanomagnets, arrays, hysteresis, cobalt

1-Introduction

Due to the potential applications in ultra-high-density magnetic recording medium, two-dimensional arrays containing rings, particles, wires and dots have attracted much attention [1-5]. Currently, ferromagnetic arrays are fabricated with advanced lithographic techniques [6-8] and characterized by magnetic force microscopy [9,10]. The ring geometry has been found to be an excellent candidate for the magnetic random access memory because the vortex state in circular rings is stable and easy to control when they are narrow [11-23]. For example, the role of the magnetic interactions in chains formed by touching rings was experimentally investigated by Welp et al. [24]. They found that the switching occurs in a pair-wise manner when the external magnetic fields are applied in-plane and perpendicular to the chain direction. This coupling introduces a broad distribution of switching fields and corresponds to a broad magnetization loop. Thus, the switching for both the isolated and the coupled rings occurs through the formation of a buckled state and the nucleation and propagation of a vortex domain wall. Adeyeye et al. [25] also experimentally studied the effects of magnetostatic interactions and film thickness on the switching of properties and reversal mechanisms of periodic arrays of elongated $\text{Ni}_{80}\text{Fe}_{20}$ thin film rings. They showed that the inter-ring spacing strongly affects not only the magnetization reversal process and the switching field distributions but also the transition fields between different equilibrium states. For example, in the case of closely packed ring arrays, sharp transitions were observed from the onion-to-vortex state due to collective magnetization reversal of the rings [25]. They also found that the range of stability of the vortex state is smaller for closely packed ring arrays compared with isolated rings of similar lateral dimensions [25]. Kaur et al. [26] fabricated ring nanostructures from ultrathin Co/Pd multilayers. MFM characterization at room temperature showed that the magnetization orientation and domain structures of nanorings were completely magnetized to saturation. The demagnetized state obtained at zero magnetic field probably consisted in a random orientation of spins on each nanostructure [26]. Recently, Edgcombe et al. [27] reported holographic measurements and compared the results with Aharonov–Bohm theory on magnetized cobalt rings; they found both onion and vortex having stable states of magnetization. Wang et al. [28] explained via micromagnetic simulations the MOKE and MFM experimental results obtained from sub-100 nm asymmetrical rings. They observed onion reverse, vortex and onion states

during the reversal magnetization. In the case of the ring diameter with very small lateral dimension (30 nm), the vortex state is still presented. Using MOKE and MFM characterization techniques, Ren et al. [29] also studied bi-ring structures. They investigated the effects of the coupling mechanism on the magnetic states and reversal processes when the rings are overlapping, connected and closely spaced. For example, when the rings are overlapped, a metastable magnetization appears due to the vortex chirality of each ring being opposite. However, micromagnetic simulations showed that both same-chirality and opposite-chirality vortex states are possible. To interpret and understand the experimental results, several theoretical studies have been performed to model magnetic nanoring arrangements. For example, Ye et al. [30] investigated two structure models of cobalt nanoring cells (double-nanorings and four-nanorings) using Monte Carlo simulation. The competition between exchange energy and dipolar energy in Co nanorings system was used to explain the emergence deviation of the vortex-type states in the connected regions. Zhang et al. [31] also investigated magnetization reversal processes of magnetic nanorings using the Monte Carlo simulation technique combined with scaling method. They presented a phase diagram for magnetic nanorings with different sizes and radius. In this interesting work, they identified three new types of magnetization reversal processes, namely, an out-of-plane onion state, a twisted triple configuration and a twisted double state. Very recently, using micromagnetic simulations Bickel et al. [32] investigated the formation of 360° domain walls created by the application of a circular magnetic field in ferromagnetic nanorings. The symmetry of the ring as the position of the circular magnetic field was the main parameter to produce the number of domain walls.

To deepen the study of the formation of the different magnetic states formed when an array of nanomagnetic rings is affected by a magnetic field, we investigated double-ring and double-dot arrays using micromagnetic simulations. The hysteresis loops were systematically calculated as a function of the thickness and the inter-nanomagnets distance. The nucleation of different magnetic states, such as vortex, twisted, and onion states and the state named cardioid [33], are analyzed in detail. In the following, the method of calculation and results are presented. The importance of this system for magnetic recording is discussed.

2-Method of calculations

Micromagnetic simulation studies were performed with emphasis on the magnetization reversal processes and the magnetization configurations in magnetic materials. To study the magnetic behavior of double cobalt nanorings and double cobalt nanodots, we use the micromagnetic theory that is based in the total magnetic energy (E). In our simulations, the exchange energy, magneto-crystalline anisotropy energy, magnetostatic energy and the Zeeman energy are taken into account. The effective magnetic field inside the ferromagnetic materials is given by: $H_{\text{effm}} = -(\partial E/\partial M)$, where M is the total magnetization. The total magnetization orientation follows the Landau-Lifshitz-Gilbert equation:

$$\frac{dM}{dt} = \frac{-\omega}{1 + \lambda^2} M \times H_{\text{eff}} - \frac{\lambda\omega}{(1 + \lambda^2)M_s} M \times (M \times H_{\text{eff}})$$

where ω is the gyromagnetic ratio, and λ is the damping coefficient. The simulation parameters are: damping constant of $\lambda = 0.5$, and M_s is the saturation magnetization of cobalt (1400×10^3 A/m). An exchange coupling constant of $A_{\text{exc}} = 1.4 \times 10^{-11}$ J/m was used to calculate the exchange energy. The magnetic anisotropy constant (K_1) was taken as zero (polycrystalline cobalt). Note that, in the fabrication of magnetic rings, regardless of the configuration, the effects of anisotropy are always present, mainly due to the grains of large sizes being almost always present. However, if the manufacturing process is precise enough such that the grain size is small, then these effects can be reduced considerably and the experimental results could be compared with the theoretical ones. To solve the Landau-Lifshitz-Gilbert equation, the finite difference method is used. Our calculations were performed using Oriented Object Micro Magnetic Frame (OOMMF) software [34,35]. A size mesh of 2 nm was used.

3-Results and discussion

Before presenting the results of the double-nanomagnets array, the magnetic properties of the single cobalt nanorings and dots are discussed. In the case of ring structures, two widths are considered: 40 and 75 nm. These structures correspond to a large and small central hole in a dot. Figure 1 shows the hysteresis loop results for nanorings with a diameter of 200 nm for different values of the thickness ($t = 2-12$ nm) and internal diameter (0, 25 and 60 nm), where internal diameter equal zero is a single

dot. Nanorings with width of 40 nm exhibit large coercive fields for $t < 10$ nm (see first column in figure 1). However, several switching of states corresponding to different spin configurations were also obtained. For example, in the case of $t \leq 4$ nm, a distorted onion state appears as a remanent state, and when the magnetic field is increased, the twisted state (metastable state, containing a 360° wall), double twisted, cardioid and reversed onion states appeared. For $t = 6$ and 8 nm, the double twisted state disappears, and only the simple twisted state at low magnetic field following a counter-clockwise curling magnetization remains. It was also found that the vortex state or curling magnetization becomes a remanent state (stable at zero magnetic field) for $t \geq 10$ nm. If $t \leq 6$ nm and the width of the nanoring is 75 nm (see second column in figure 1), which corresponds to a small hole in the magnetic dot, we found that the reversal magnetization is achieved by means of the sequence onion-twisted and reversed onion states. For these values of thickness, the twisted state appears as a remanent state. For $t = 8$ nm, the system exhibits a reversal magnetization by means of the sequence onion-twisted-vortex states, but the twisted state remains as the remanent state. For even larger values of the thickness ($t > 8$ nm), the onion and vortex states only remained in the hysteresis loops; in addition, the vortex state becomes stable at zero magnetic fields. The cobalt magnetic dot results (see third column in figure 1) indicate the presence of single domain states if $t \leq 6$ nm. Here, the reversal magnetization is achieved by means of the sequence onion and reversal onion state. In the case of $t = 8$ nm, a metastable vortex state appears, but its central core changes with the increment of the magnetic field. This core is moved vertically, perpendicular to the applied magnetic field. This vortex state becomes the remanent state up to $t = 20$ nm.

Figure 2 shows the hysteresis loops for the cobalt double nanorings when they are in contact (first column) and when they are separated by 50 nm (second column); here, different values of the thickness are shown ($t = 2-20$ nm). In the first case, for low values of the thickness ($t = 2-8$ nm), the systems exhibit a strong interactions between the rings avoiding the vortex state nucleation. In the case of the rings separated by 50 nm and $t = 2-6$ nm, we observe the onion, twisted, cardioid, vortex states and their combinations. It was found that the first switching in the magnetization is given via a closure magnetization when $t \geq 12$ nm and $t \geq 8$ nm for rings in contact and rings separated, respectively. For the in-contact rings, the left (right) ring exhibits a clockwise (counter-clockwise)

closure magnetization. In the 50-nm-separation D-rings, for $t = 10$ nm, both rings exhibit a clockwise closure magnetization, while for $t = 12-18$ nm, the left (right) ring exhibits a counter-clockwise (clockwise) closure magnetization, and for $t = 20$ nm the system recovers the behavior observed in $t = 10$ nm. An additional intermediate switching is observed in the 50-nm-separation D-rings with $t = 12-18$ nm. This intermediate switching was not observed in the other cases. In this intermediate state, the system exhibits a clockwise closure magnetization state only in the right ring. In both of the inter-rings distances analyzed, the hysteresis loops became more extended, giving a last switching at higher fields. Note that, for intermediate values of the thickness, the system can change the sense of the curling magnetization, as observed in the D-rings separated by 50 nm. For the thin rings ($t \leq 8$ nm), the system exhibits more complex magnetization states (twisted, distorted onion, or cardioid states). A detailed magnetic states description in the hysteresis loop with $t = 4$ nm for touching nanorings is shown in figure 3, which exhibits the results on the spin configurations in different magnetic fields for thin D-rings of touching nanorings with thickness of 4 nm.

The hysteresis loops for two interacting nanorings with a width of 75 nm and thicknesses from 2 to 20 nm are shown in figure 4. The left column shows the results when they are not separated (in contact nanorings), whereas the right side in figure 4 depicts results for the 50-nm inter-ring distance. In the case of touching nanorings, with small thickness values ($t = 2-6$ nm), the reversal magnetization is achieved via the motion of the onion state around the nanoring until the twisted state is emerging. Similar trends were observed for nanorings separated by 50 nm, but in this case, the reversal magnetization is driven by the twisted state. For in-contact nanorings with $t = 8$ nm, the onion, twisted, and cardioid states nucleation were observed. In the case of nanorings separated by 50 nm and the same thickness of $t = 8$ nm, we observed several switching fields: the second switching in the magnetization is given via a counter-clockwise closure magnetization in the left ring, while the right one exhibits a twisted state. In the zero-nm-separation D-rings, for $t = 12-14$ nm, the left (right) rings exhibit a counter-clockwise (clockwise) closure magnetization, and for rings separated 50 nm and $t = 10-16$ nm, their behavior is identical. For thicknesses from 16-20 nm in both rings, a vortex state with counter clockwise closure magnetization appears, while in the rings separated 50 nm, the

flux vortex is clockwise.

The results on the magnetic patterns in different magnetic fields for wider D-ring of touching nanorings with a thickness of 4 nm are shown in figure 5. We observe in the hysteresis loop that reversal magnetization is due to onion and twisted states nucleation. The inset in figure 5 shows the role of exchange and demagnetization energies during magnetic configurations nucleation. The exchange energy contribution is always dominated along the hysteresis loop.

Figure 6 displays the hysteresis loops of double-dot arrays for the cases of in contact and separated by 50-nm dots. In both arrays, we observe squared loops with weak coercive fields for thicknesses of 2-6 nm; here, the magnetization reversal is driven by the nucleation of magnetic states type-C. For in-contact dots and $t = 8$ nm, the magnetization reversal is achieved by means of a vortex state (left dot) and a type-S state (right dot). For separated dots and $t = 8$ nm, more steps in the hysteresis loop are observed; hence, around zero magnetic field, both dots exhibit a vortex state. For $t = 10$ -20 nm, in both arrays (in contact dots and separated dots by 50 nm), the magnetization reversal is driven by the vortex state nucleation, which is identified by the linear behavior of the hysteresis loop around a zero magnetic field. Notice that the magnetic field range, where the linear behavior emerges, increases with the thickness. Figure 7 shows the different magnetic states along the hysteresis loop for touching dots with a thickness of $t = 20$ nm. Notice that the magnetization reversal is achieved by the vortex state nucleation (counter clockwise), which is propagated perpendicularly to the magnetic field direction passing by the dot center (see the spin configurations, labels “b-e”). Notice that the magnetostatic energy contribution around zero magnetic field is dominant where both rings exhibit a vortex state (see inset figure 7).

4- Conclusions

We studied the magnetization of double-nanomagnet arrays formed by cobalt nanorings and dots with different thickness using micromagnetic simulations. The hysteresis loops were calculated under the action of an external magnetic field applied in the plane. The effects of thickness and the inter-magnets distance on the magnetic behavior were systematically presented. In particular, we observed

the presence of both twisted and cardioid states with large stabilities. Furthermore, two twisted states coexisted with an onion state. Arrays of circular nanorings show diverse magnetic spin configurations, particularly the double twisted and cardioid states, which were not found in isolated cases. In these cases, the reversal magnetization in a single narrow ring is achieved via the onion state followed by a perfect vortex state for $t \geq 12$ nm. The hysteresis loops for D-rings with wide rings exhibit multiple steps when the rings are in contact, whereas, for 50-nm inter-rings separation, the reversal magnetization is obtained via the onion state followed by vortices states for $t \geq 10$ nm. For a single wide ring, the hysteresis loops exhibit multiple states for $t \leq 8$ nm, and two types of magnetic states are found for $t \geq 10$ nm (onion state followed by vortex states). The results for D-dots exhibit squared hysteresis loops for $t \leq 6$ nm (single-domain transition), regardless of the inter-magnets separation, whereas the single dot exhibits single domain transition for $t \leq 6$ nm. Double-nanomagnet arrays of Co nanorings present diverse magnetic configuration that can be used to fabricate ultra-high-density magnetic recording devices.

Acknowledgments

The authors are grateful to G. J. Labrada-Delgado, B. A. Rivera-Escoto, and K. Gomez for their technical assistance. This work was partially supported by CONACYT-México grants: 60218-F1 (FLU) and CB-2013-220744. JJTH gratefully acknowledges the support from ITSCH.

References

1. J.-G. Zhu, Y. Zheng, G. A. Prinz, Ultrahigh density vertical magnetoresistive random access memory, *J. Appl. Phys.* 87 (2000) 6668.
2. X. F. Han, Z. C. Wen, H. X. Wei, Nanoring magnetic tunnel junction and its application in magnetic random access memory demo devices with spin-polarized current switching, *J. Appl. Phys.* 103 (2008) 07E933.
3. K. Nielsch, R. B. Wehrspohn, J. Barthel, J. Kischner, U. Gosele, S. F. Fischer, H. Kronmuller, Hexagonally ordered 100 nm period nickel nanowire arrays, *Appl. Phys. Lett.* 79 (2001) 1360.
4. U. Welp, V. K. Vlasko-Vlasov, G. W. Crabtree, J. Hiller, N. Zaluzec, V. Metlushko, B. Ilic, Magnetization reversal in arrays of individual and coupled Co-rings, *J. Appl. Phys.* 93 (2003) 7056.

5. C. A. Ross, M. Hwang, M. Shima, J. Y. Cheng, M. Farhoud, T. A. Savas, Henry I. Smith, W. Schwarzhacher, F. M. Ross, M. Redjhal, F. B. Humphrey, Micromagnetic behaviour of electrodeposited cylinder arrays, *Phys. Rev. B* 65 (2002) 144417.
6. L. J. Heyderman, C. David, M. Kläui, C. A. F. Vaz, J. A. C. Bland, Nanoscale ferromagnetic rings fabricated by electron-beam lithography, *J. Appl. Phys.* 93 (2003) 10011.
7. A. Kosiorek, Witold Kandulski, Hanna Glaczynska, Michael Giersig, Fabrication of Nanoscale Rings, Dots, and Rods by Combining Shadow Nanosphere Lithography and Annealed Polystyrene Nanosphere Masks, *Small* 1 (2005) 439–444.
8. K. Cho, G. Loget, R. M. Corn, Lithographically Patterned Nanoscale Electrodeposition of Plasmonic, Bimetallic, Semiconductor, Magnetic, and Polymer Nanoring Arrays, *J. Phys. Chem. C* 118 (2014) 28993–29000.
9. J. Bekaert, D. Buntinx, C. Van Haesendonck, V. V. Moshchalkov, J. De Boeck, G. Borghs, V. Metlushko, Noninvasive magnetic imaging and magnetization measurement of isolated mesoscopic Co rings, *Appl. Phys. Lett.* 81 (2002) 3413.
10. J. Li, S. Zhang, Chris, R. Misra, J. Bartell, V. H. Crespi, Peter Schiffer, Magnetization states and switching in narrow-gapped ferromagnetic nanorings, *AIP Advances* 2 (2012) 012136.
11. M. Hanson, O. Kazakova, P. Blomqvist, R. Wäppling, B. Nilson, Magnetic domain structures in submicron-size particles of epitaxial Fe (001) films: Shape anisotropy and thickness dependence, *Phys. Rev. B* 66 (2002) 144419.
12. T. Shinjo, T. Okuno, R. Hassdorf, K. Shigeto, T. Ono, Magnetic Vortex Core Observation in Circular Dots of Permalloy, *Science* 289 (2000) 930.
13. M. Kläui, C. A. F. Vaz, L. Lopez-Diaz and J. A. C. Bland, Vortex formation in narrow ferromagnetic rings, *J. Phys.: Condens. Matter* 15 (2003) R985.
14. R. P. Cowburn, A. O. Adeyeye, M. E. Welland, Configurational Anisotropy in Nanomagnets, *Phys. Rev. Lett.* 81 (1998) 5414.
15. P. Vavassori, M. Grimsditch, V. Novosad, V. Metlushko and B. Ilic, Metastable states during magnetization reversal in square permalloy ring, *Phys. Rev. B* 67 (2003) 134429.
16. J. Rothman, M. Kläui, L. Lopez-Diaz, C. A. F. Vaz, A. Bleloch, J. A. C. Bland, Z. Cui, R. Speaks, Observation of a Bi-Domain State and Nucleation Free Switching in Mesoscopic Ring Magnets, *Phys. Rev. Lett.* 86 (2001) 1098.
17. L. Lopez-Diaz, J. Rothman, M. Kläui and J. A. C. Bland, Vortex formation in magnetic narrow rings: The role of magneto-crystalline anisotropy, *J. Appl. Phys.* 89 (2001) 7579.
18. M. Kläui, J. Rothman, L. Lopez-Diaz, C. A. F. Vaz, J. A. C. Bland, Z. Cui, Vortex circulation control in mesoscopic ring magnets, *Appl. Phys. Lett.* 78 (2001) 3268.
19. F. J. Castaño, C.A. Ross, C. Frandsen, A. Eilez, D. Gil, H. I. Smith, M. Redjal, F.B. Humphrey, Metastable states in magnetic nanorings, *Phys. Rev. B* 67 (2003) 184425.
20. J. K. Ha, R. Hertel, J. Kirschner, Micromagnetic study of magnetic configurations in submicron permalloy disks, *Phys. Rev. B* 67 (2003) 224432.

21. R. P. Cowburn, M. E. Welland, Phase transitions in planar magnetic nanostructures, *Appl. Phys. Lett.* 72 (1998) 2041.
22. T. Pokhil, D. Song, J. Nowak, Spin vortex states and hysteretic properties of submicron size NiFe elements, *J. Appl. Phys.* 87 (2000) 6319.
23. X. Wang, I. Purnama, M. C. Sekhar, W. S. Lew, Highly Stable Vortex State in Sub-100 nm Nanomagnets, *Appl. Phys. Express* 5 (2012) 053001.
24. U. Welp, V. K. Vlasko-Vlasov, J. M. Hiller, N. J. Zaluzec, V. Metlushko, B. Ilic, Magnetization reversal in arrays of Co rings, *Phys. Rev. B* 68 (2003) 054408.
25. A. O. Adeyeye, S. Goolaup, N. Singh, C. C. Wang, X. S. Gao, C. A. Ross, W. Jung, F. J. Castaño, Magnetostatic coupling in arrays of elongated Ni₈₀Fe₂₀ rings, *J. Phys. D: Appl. Phys.* 40 (2007) 6479–6483.
26. M. Kaur, M. Raju, D. Varandani, A. Gupta, T. D. Senguttuvan, B. R. Mehta, R. C. Budhani, Reversal and thermal stability of ordered moments in nano-rings of perpendicular anisotropy Co/Pd multilayers, *J. Phys. D: Appl. Phys.* 48 (2015) 295005.
27. C. J. Edgcombe, A. Ionescu, J. C. Loudon, A. M. Blackburn, H. Kurebayashi, C. H. W. Barnes. Characterisation of ferromagnetic rings for Zernike phase plates using the Aharonov–Bohm effect. *Ultramicroscopy* 120 (2012) 78.
28. X. Wang, I. Purnama, M. C. Sekhar, W. S. Lew, Highly Stable Vortex State in Sub-100 nm Nanomagnets, *Appl. Phys. Express* 5 (2012) 053001
29. Y. Ren, S. Jain, A. O. Adeyeye, C. A. Ross, Magnetization states in coupled Ni₈₀Fe₂₀ bi-ring nanostructures, *New J. Phys.* 12 (2010) 093003.
30. Q. Ye, S. Chen, K. Zhong, Z. Huang, Magnetic properties for cobalt nanorings: Monte Carlo simulation, *Physica B* 407 (2012) 790–794.
31. W. Zhang, S. Haas, Phase diagram of magnetization reversal processes in nanorings, *Phys. Rev. B* 81, (2010) 064433.
32. J. E. Bickel, S. A. Smith, K. E. Aidala, The creation of 360° domain walls in ferromagnetic nanorings by circular applied magnetic fields, *J. Appl. Phys.* 115 (2014) 17D135.
33. J. J. Torres-Heredia, E. Munoz-Sandoval, F. López-Urías. Micromagnetic simulation of Fe nanorings. *J. Magn. Magn. Matter.* 294 (2005) E1-5
34. R. D. McMichael, M. J. Donahue, Head to head domain wall structures in thin magnetic strips, *IEEE Trans. Magn.* 33 (5) (1997) 4167.
35. M. J. Donahue, D. G. Porter, OOMMF User'Guide, version 1.0, Interagency Report NISTIR 6376 (2004).

FIGURES AND CAPTIONS

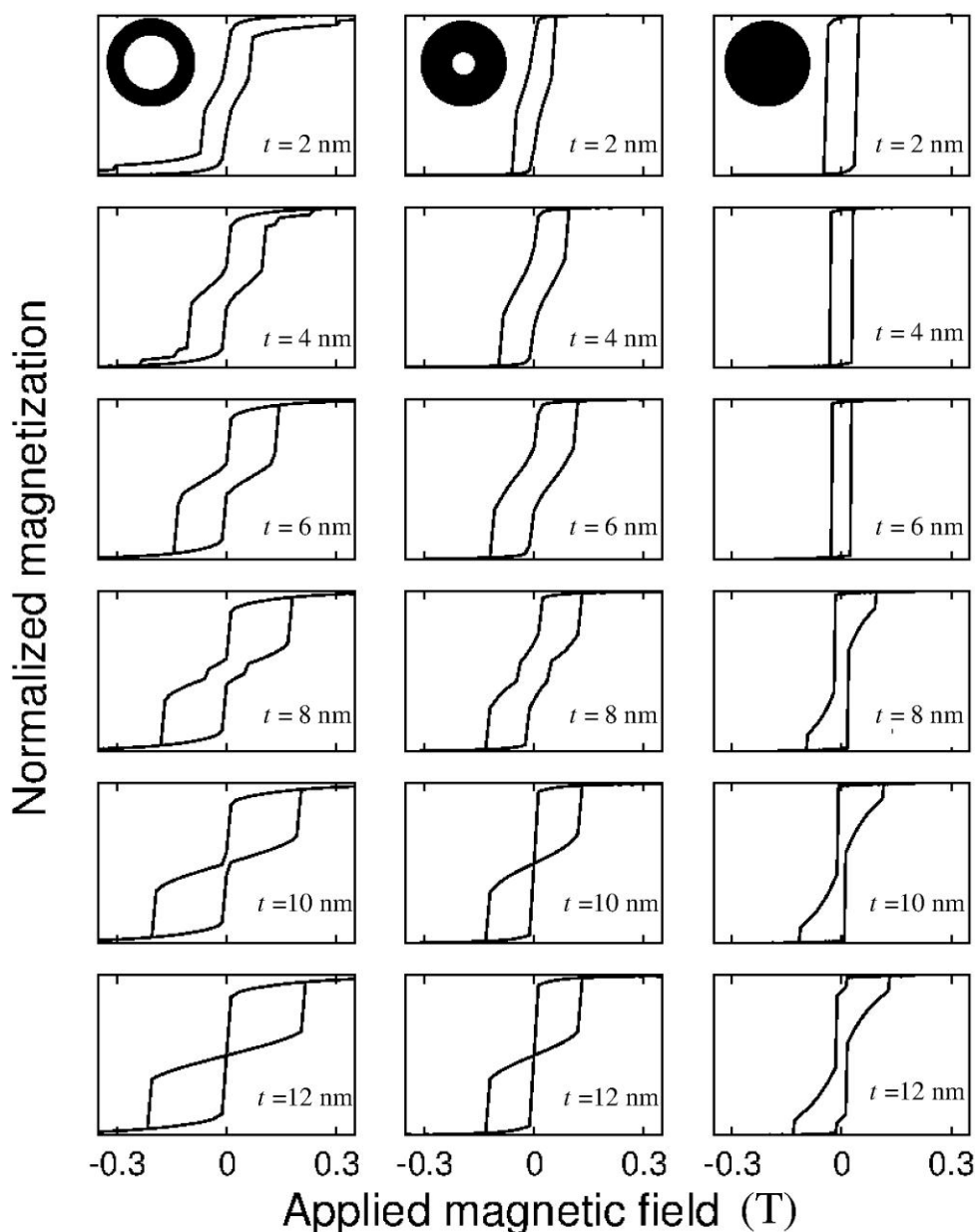


Figure 1: Hysteresis loops for individual cobalt nanorings with a width of 40 nm (narrow) and 75 nm (wide) in the first and second columns, respectively, and for dots (third column). Different values of the thickness are displayed ($t = 2$ -12 nm). All nanomagnets have a diameter of 200 nm. The external magnetic field is applied in plane. Notice that the thin and narrow nanorings ($w = 40$ nm and $t \leq 4$ nm) exhibit multi-switching hysteresis loops, whereas the dot exhibits a single domain reversal magnetization (squared loop) for $t \leq 6$ nm. In both nanorings and dots, the vortex spin configuration appears for $t \geq 8$ nm; however, this becomes the remanent state for $t \geq 12$ nm.

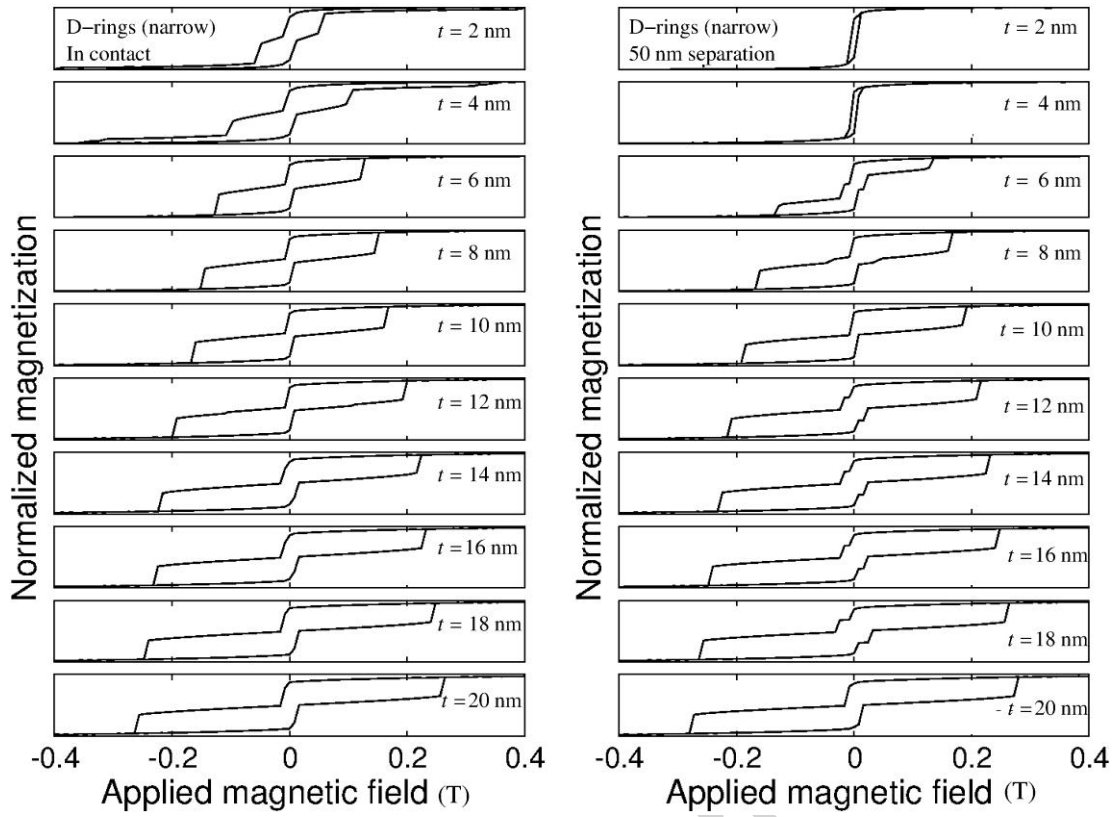


Figure 2: Hysteresis loops for double narrow cobalt nanorings in contact (first column) and separated by 50 nm (second column) for different thicknesses ($t = 2$ - 20 nm). Each ring has 200 nm of diameter and a width of 40 nm. The external magnetic field is applied in plane. Note that for 50-nm separation rings (right column), the hysteresis loops exhibit an intermediate switching for $12 \leq t \leq 18$ nm that corresponds to the coexistence between the onion state (left ring) and twisted state (right ring).

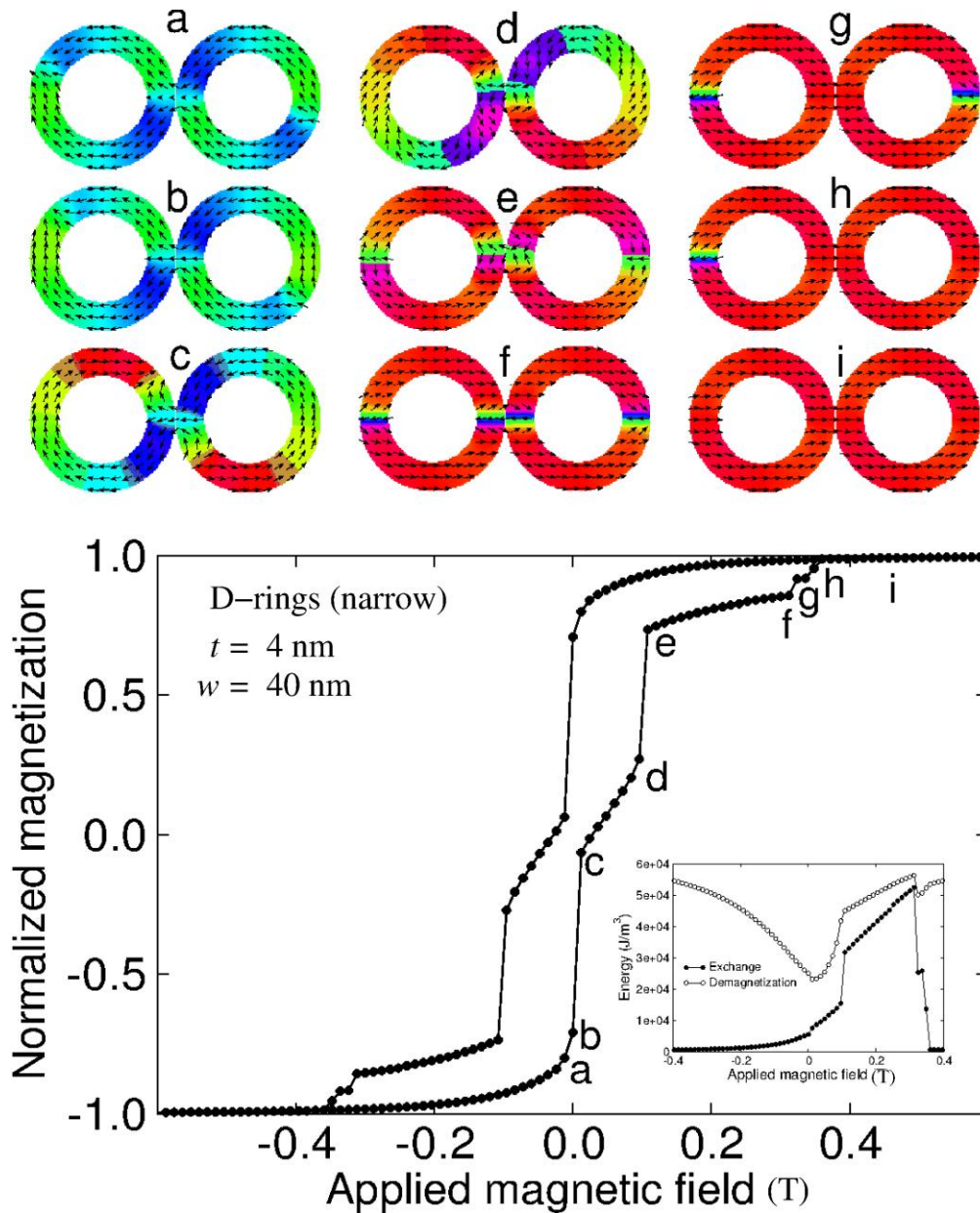


Figure 3: (Color online) Hysteresis loop for double (D-rings) cobalt nanorings in contact and a thickness of 4 nm. Each nanoring has 200 nm of diameter. The magnetization patterns of the different labels of the curve are displayed in the top part. The external magnetic field is applied in plane. The inset shows the exchange and the demagnetization energies. The labels "a" and "b" correspond to the onion states and "c" and "d" are the twisted states with 360° domain wall in the nearest parts of the rings. The labels "e" to "f" represents a bidomain state with two types of domain wall. Here, the right ring exhibits a cardioid state in its right side, while the other domain walls correspond to the twisted state with 180° . The label "g" represents a coexistence of the twisted (left ring) and cardioid (right ring) states. The label "h" is a twisted state in the left ring. The saturated state is displayed in label "i".

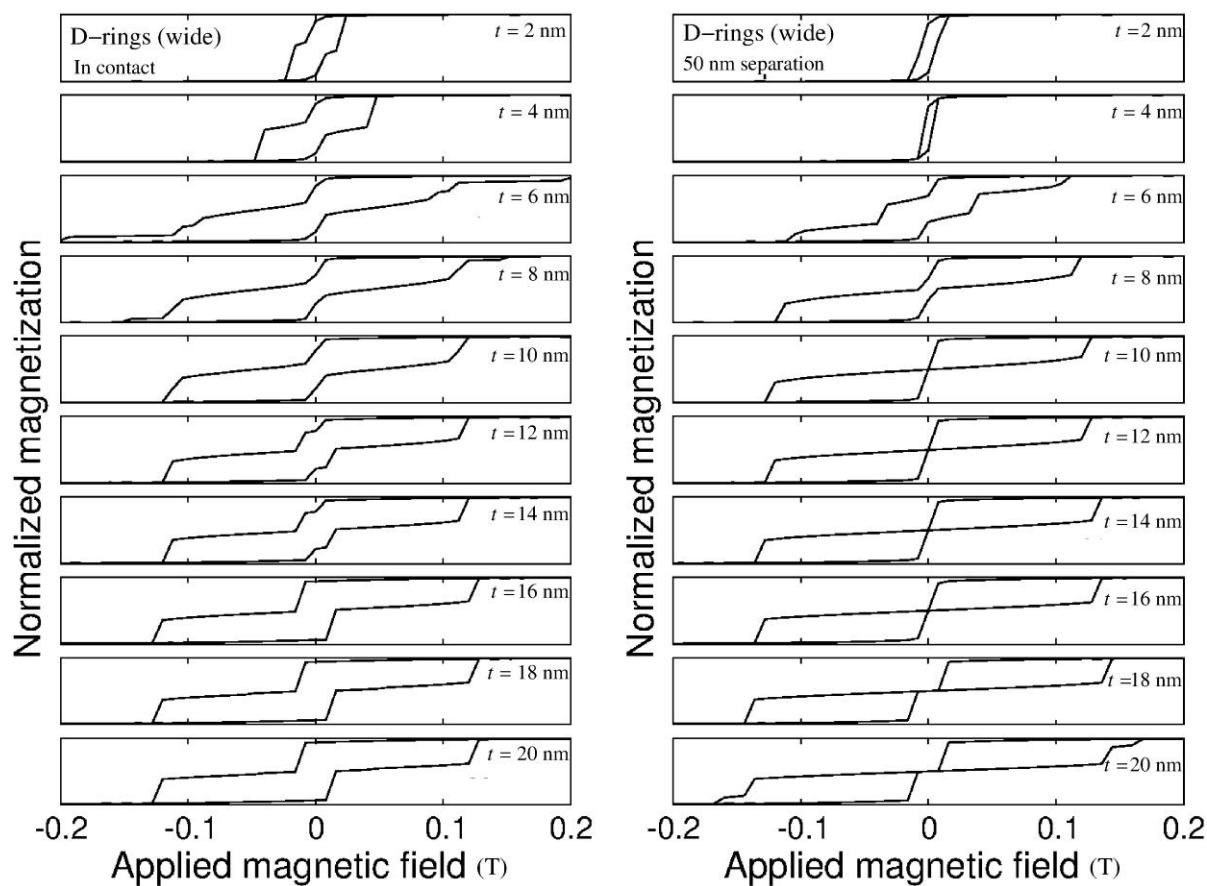


Figure 4: Hysteresis loops for wide (75 nm) double cobalt nanorings in contact (first column) and 50-nm separation (second column) for different thicknesses ($t = 2$ -20 nm). Each nanoring has a diameter of 200 nm. The external magnetic field is applied in plane.

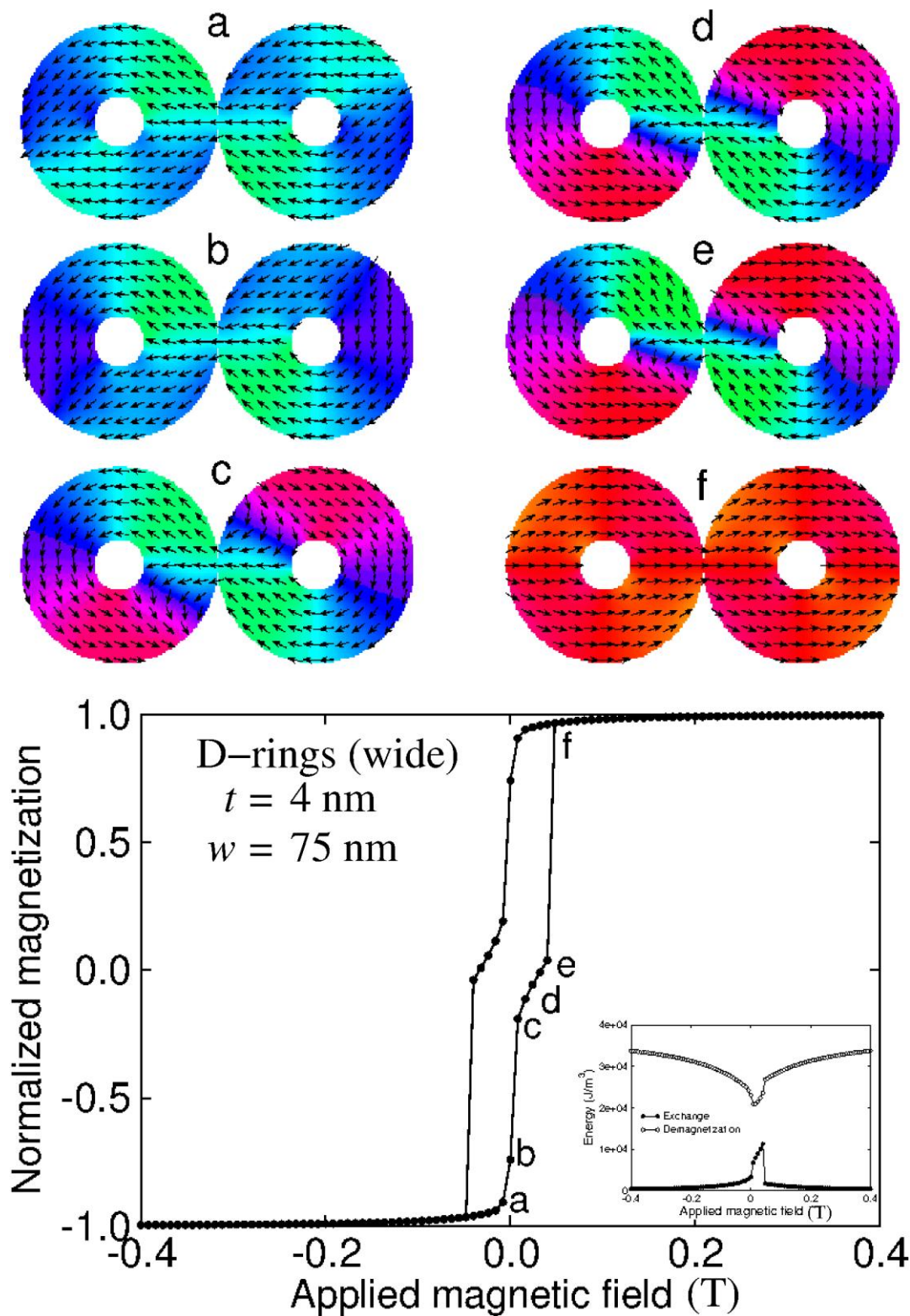


Figure 5: (Color online) Hysteresis loop for D-rings array. The nanorings are in contact, which presents a width of 75 nm and a thickness of 4 nm. The individual nanoring has a diameter of 200 nm. The magnetization patterns of the different labels of the curve are displayed in the top part. The external magnetic field is applied in plane. The inset shows the corresponding exchange and demagnetization energies.

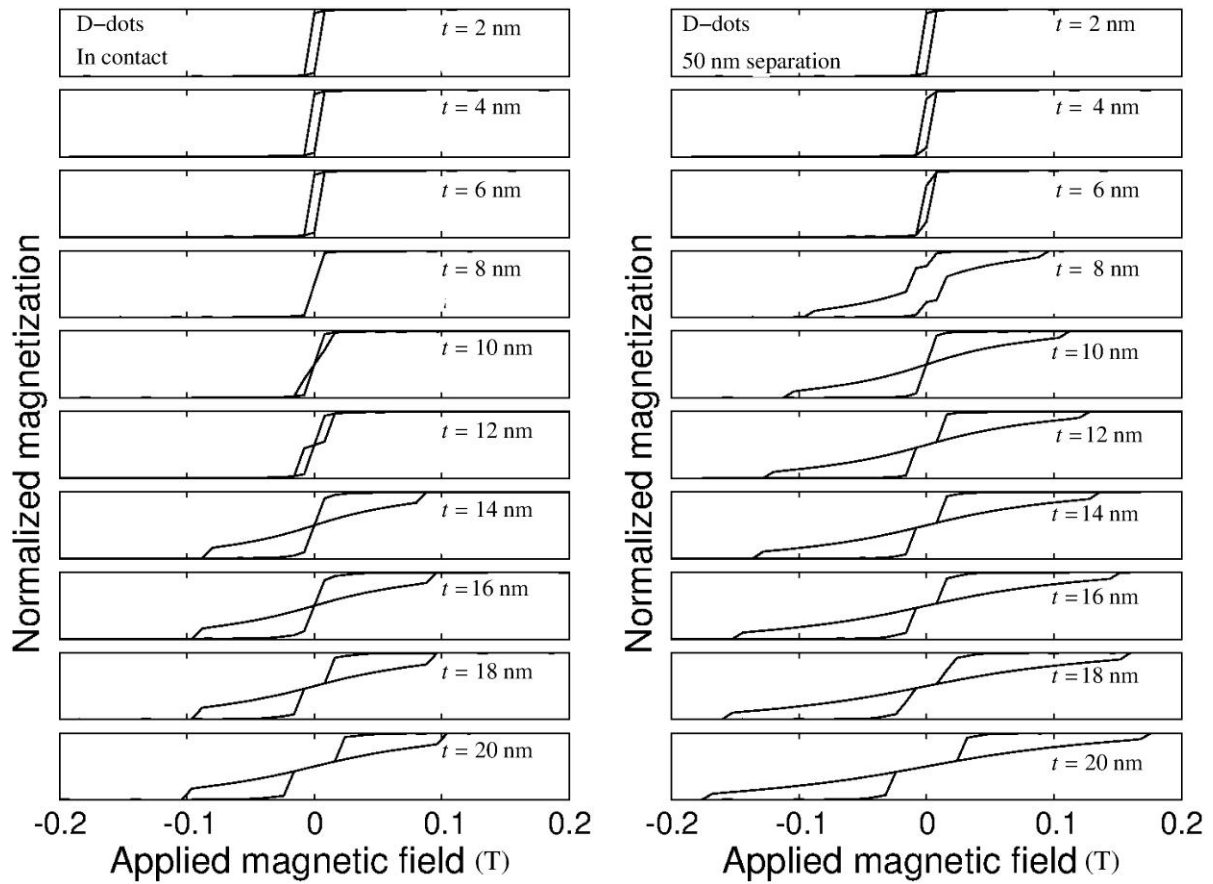


Figure 6: Hysteresis loops for in contact double dots (D-dots) in the first column and 50-nm separation in the second column for different values of the thickness ($t = 2-20$ nm). Each dot has a diameter of 200 nm. The external magnetic field is applied in plane

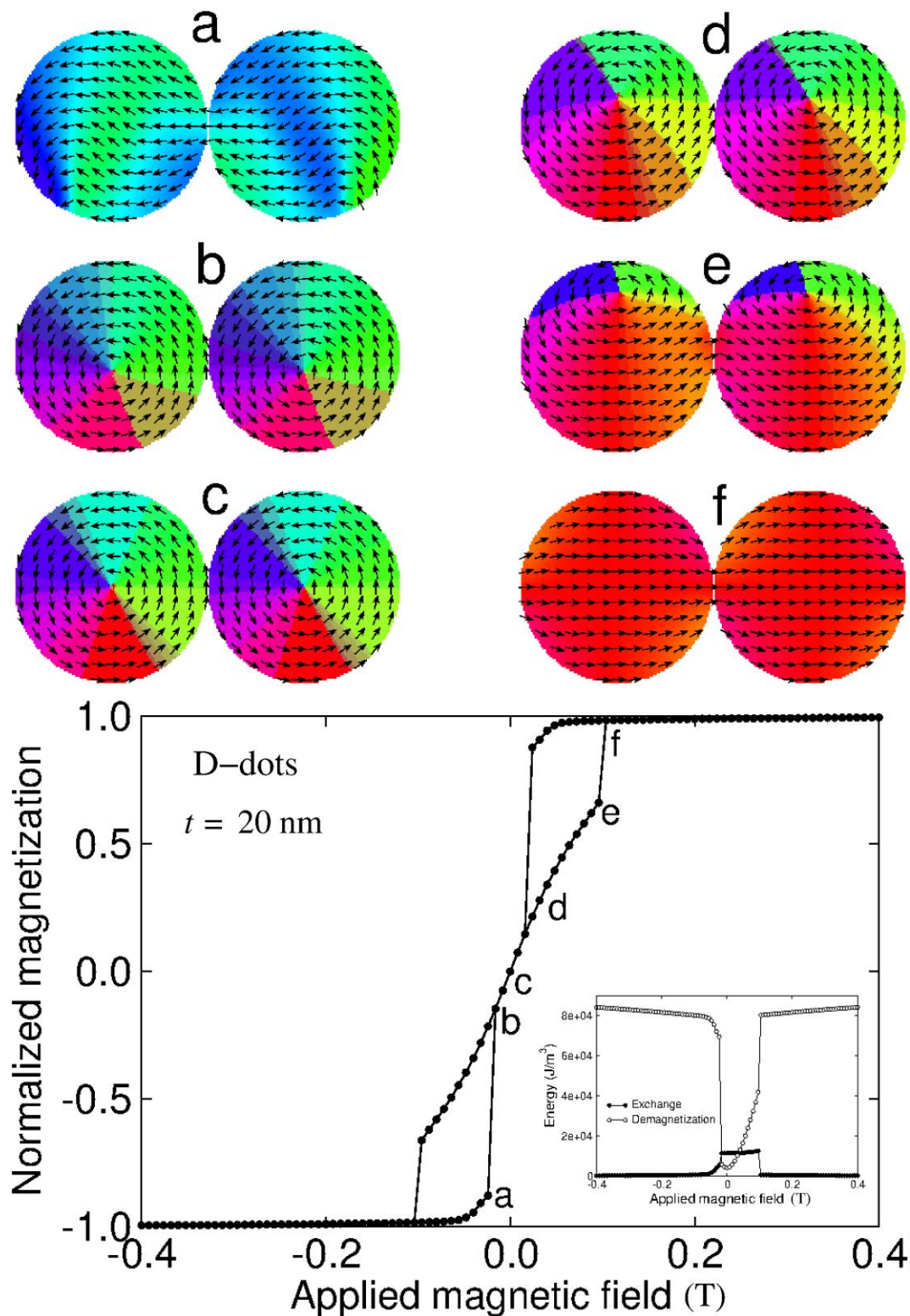


Figure 7: (Color online) Hysteresis loop of cobalt double-dot (D-dots) with zero separation and a thickness of 20 nm. The individual dots have a diameter of 200 nm. The magnetization patterns associated with different fields labeled by a-f are displayed in the top part. The external magnetic field is applied in plane. The inset shows the corresponding exchange and demagnetization energies.